Int. J. Heat Mass Transfer. Vol. 35, No. 2, pp. 403–420, 1992
Printed in Great Britain

0017–9310/92 $5.00 + 0.00

The Reynolds-stress model of turbulence applied to the natural-convection boundary layer along a heated vertical plate

T. W. J. PEETERS and R. A. W. M. HENKES

Group Transport Phenomena, Section Heat Transfer, Faculty of Applied Physics, Delft University of Technology, P.O. Box 5046, 2600 GA Delft, The Netherlands

(*Received* 9 *April* 1990 *and in final form* 20 *September* 1990)

Abstract—The turbulent natural-convection boundary layer for air along a heated vertical plate is investigated numerically with an algebraic (ASM) and fully differential Reynolds-stress model (RSM). From the literature a set of model constants is selected, in such a way that the wall-heat transfer and mean-flow structure are predicted in close agreement with the experimental data. Sensitivity tests on RSM constants show which constants dominate the mean-flow prediction, and which constants only affect turbulence quantities. Wall modifications are employed to improve predictions of the near-wall turbulence. RSM calculations of the turbulence quantities agree well with available experimental data. ASM results are poorer, but still in qualitative agreement with experiments. Hence, in natural-convection boundary layers, the local-equilibrium assumption has only limited applicability. Furthermore, the eddy-viscosity concept used in the k–ε model (KEM) is tested. The KEM gives good mean-flow results, but for a good prediction of the detailed turbulence structure the RSM is needed.

1. INTRODUCTION

TO SOLVE turbulent flow problems in complex geometries, the Reynolds-stress model is often needed in cases where the well-known k–ε model (KEM) fails to give accurate results. To obtain a generally applicable turbulence model the Reynolds-stress model has to be tested for simple geometries as well: the present paper gives Reynolds-stress calculations for the turbulent natural-convection boundary layer for air along a heated vertical plate.

For this geometry, it is not expected that the Reynolds-stress model will yield a significantly better prediction of the mean-flow characteristics than existing k–ε models. Henkes and Hoogendoorn [1] found several low-Reynolds-number k–ε models to perform very well. In particular, the models of Jones and Launder [2], Chien [3] and Lam and Bremhorst [4] predict the wall-heat transfer within experimental uncertainty. For the present flow geometry, the Reynolds-stress model can provide a better understanding of near-wall turbulence and it can show whether KEM assumptions hold.

In the literature on Reynolds-stress modeling there is still no agreement on the right wall modifications and incorporation of anisotropy. The selected model closely resembles the model recommended by To and Humphrey [5], who used an algebraic stress model (ASM) for the natural-convection boundary layer. Shortcomings of their model were the omission of an important term in the ε equation (see ref. [1]) and the assumption of local equilibrium for the Reynolds stresses. We carried out calculations with an ASM and a fully differential stress model (RSM), which clearly show that the local-equilibrium assumption is not valid for this type of flow. To obtain better predictions of the near-wall region, modification functions are derived and incorporated in the RSM equations.

The influence of model constants on the RSM results is tested by a sensitivity analysis. ASM and RSM calculations are compared with experimental data of Miyamoto *et al.* [6] and Tsuji and Nagano [7–9]. This comparison shows that the fully differential RSM is superior to the ASM for this type of flow.

The KEM uses the eddy-viscosity concept to model the Reynolds stress and the turbulent heat fluxes. This concept describes turbulence as a diffusion process, with the aid of a local isotropic turbulent viscosity. A strict analogy between Reynolds stresses and turbulent heat fluxes is assumed, as expressed by the turbulent Prandtl number σ_θ, which is a constant in the KEM. The eddy-viscosity concept gives isotropic turbulent intensities, i.e. $\overline{u_i'^2} = \frac{2}{3}k$, $i = 1, 2, 3$. Furthermore, the turbulent flux vector $-\overline{u_i'\phi'}$ for a quantity ϕ is assumed to have the same direction as the mean-gradient vector of ϕ. Thus, the eddy-viscosity concept cannot distinguish between anisotropy and inhomogeneity of the turbulence. Our calculations will show that some of the assumptions in the eddy-viscosity concept do not hold in the natural-convection boundary layer.

2. REYNOLDS-STRESS MODELING

2.1. *Reynolds-stress equation*

The partial differential equations describing transport of Reynolds stresses $\overline{u_i'u_j'}$ can be derived from the

NOMENCLATURE

c_p	specific heat at constant pressure [J kg^{-1} K^{-1}]
g	gravitational acceleration (=9.81 m s^{-2})
Gr_x	local Grashof number, $g\beta\Delta\Theta x^3/\nu^2$
k	turbulent kinetic energy [J kg^{-1}]
Nu_x	local Nusselt number, $x/\Delta\Theta(\partial\Theta/\partial y)_w$
Pr	Prandtl number, $\rho\nu c_p/\lambda$
Re	Reynolds number, $x_{ref}u_{ref}/\nu_{ref}$
u, v, w	velocity components [m s^{-1}]
u_b	laminar buoyant velocity scale, $\sqrt{(g\beta\Delta\Theta x)}$ [m s^{-1}]
u_τ	friction velocity, $\sqrt{(\tau_w/\rho)}$ [m s^{-1}]
x	coordinate along plate [m]
y	coordinate perpendicular to plate [m]
y^+	dimensionless transverse coordinate, yu_τ/ν.

Greek symbols

α	thermal diffusivity, $\lambda/(\rho c_p)$ [m^2 s^{-1}]
β	coefficient of volumetric thermal expansion [K^{-1}]
$\Delta\Theta$	temperature difference, $\Theta_w-\Theta_\infty$ [K]
ε	viscous dissipation rate of turbulent kinetic energy [m^2 s^{-3}]
ε_θ	thermal dissipation rate of temperature fluctuations [K^2 s^{-1}]
ζ	dimensionless similarity coordinate, $(y/x)Nu_x$
θ	temperature [K]
Θ_τ	friction temperature, $-\alpha/u_\tau(\partial\Theta/\partial y)_w$ [K]
λ	thermal conductivity [W m^{-1} K^{-1}]
ν	kinematic viscosity [m^2 s^{-1}]
ρ	density [kg m^{-3}]
σ_ϕ	turbulent Prandtl number for quantity ϕ
τ_w	wall shear stress [N m^{-2}]
τ_m	mechanical turbulence time scale, k/ε [s]
τ_θ	thermal turbulence time scale, $\frac{1}{2}\overline{\theta'^2}/\varepsilon_\theta$ [s].

Superscripts

ϕ'	fluctuating part of quantity ϕ
$\bar{\phi}, \Phi$	time-mean part of quantity ϕ.

Subscripts

i, j, k	Cartesian coordinate directions
max	maximum value of quantity
t	turbulent quantity
w	wall condition
∞	ambient condition.

Navier–Stokes equations. For a stationary incompressible buoyant flow under the Boussinesq approximation one obtains:

$$U_k\frac{\partial\overline{u_i'u_j'}}{\partial x_k}=d_{ij}+P_{ij}+G_{ij}+\Phi_{ij}-\varepsilon_{ij} \qquad (1)$$

where

$$d_{ij}=\frac{\partial}{\partial x_k}\left(\nu\frac{\partial\overline{u_i'u_j'}}{\partial x_k}-\overline{u_i'u_j'u_k'}-\frac{\overline{p'u_i'}}{\rho}\delta_{jk}-\frac{\overline{p'u_j'}}{\rho}\delta_{ik}\right)$$

$$P_{ij}=-\left(\overline{u_i'u_k'}\frac{\partial U_j}{\partial x_k}+\overline{u_j'u_k'}\frac{\partial U_i}{\partial x_k}\right);$$

$$G_{ij}=-\beta(\overline{u_i'\theta'}g_j+\overline{u_j'\theta'}g_i)$$

$$\Phi_{ij}=\overline{\frac{p'}{\rho}\left(\frac{\partial u_i'}{\partial x_j}+\frac{\partial u_j'}{\partial x_i}\right)};\quad \varepsilon_{ij}=2\nu\overline{\frac{\partial u_i'}{\partial x_k}\frac{\partial u_j'}{\partial x_k}}.$$

The terms on the right-hand side of equation (1) represent laminar and turbulent diffusion d_{ij}, mean-shear production P_{ij}, buoyant production G_{ij}, pressure–strain correlation Φ_{ij} and viscous dissipation rate ε_{ij}. In our second-moment closure, the production/destruction terms P_{ij} and G_{ij} are known exactly. All other second- and higher-order correlations have to be modeled.

A complicated and important term in equation (1) is the pressure–strain correlation Φ_{ij}. Since $\Phi_{ii}=0$, it does not appear in the transport equation for the turbulent kinetic energy k. Hence, Φ_{ij} redistributes turbulent energy between the normal stresses, leaving k unchanged. Its influence on the Reynolds-shear stress is less evident. Theoretical analyses on the modeling of Φ_{ij} usually start with the approach given by Chou [10]. Chou used a Poisson equation for the pressure fluctuations to obtain an integral expression for Φ_{ij}, in which four different contributions can be distinguished: turbulence–turbulence interactions $\Phi_{ij}^{(1)}$, turbulence–mean flow interactions $\Phi_{ij}^{(2)}$, buoyancy effects $\Phi_{ij}^{(3)}$ and a surface integral. The latter can be neglected far enough from fixed walls, whereas the other three contributions are modeled separately.

For the turbulent part, Rotta [11] proposed a simple linear model, assuming a 'return to isotropy' proportional to the rate of anisotropy:

$$\Phi_{ij}^{(1)}=-C_1\frac{\varepsilon}{k}(\overline{u_i'u_j'}-\tfrac{2}{3}k\delta_{ij}). \qquad (2)$$

Experiments of Uberoi [12] and Tucker and Reynolds [13] on the decay of grid turbulence suggest a C_1-value of about 2.5–3.0. Lumley [14] pointed out that C_1 is not a universal constant, but depends on the turbulence Reynolds number and the rate of anisotropy. This possibly explains the large discrepancies in the literature on the correct value for C_1: Launder *et al.* [15] used $C_1=1.5$, whereas Gibson and Younis [16] took $C_1=3.0$. For buoyant flows often $C_1\approx 2.2$ is used.

The mean-strain part or rapid-distortion part $\Phi_{ij}^{(2)}$ can be written as:

$$\Phi_{ij}^{(2)} = A_{ijlm}\frac{\partial U_l}{\partial x_m} \tag{3}$$

where A_{ijlm} is a fourth-rank tensor. According to Rotta [11], A_{ijlm} should satisfy the symmetry and traceless properties of Φ_{ij}, and furthermore $A_{ijjm} = 2\overline{u_i'u_m'}$ under contraction of indices. Analogous to equation (2), Rotta proposed a simple model for the mean-strain part:

$$\Phi_{ij}^{(2)} = -C_2(P_{ij} - \tfrac{2}{3}P_k\delta_{ij}). \tag{4}$$

This model enforces an isotropization of the production tensor P_{ij}. Rotta chose $C_2 = 0.6$, adopted by many workers. Gibson and Younis [16], however, took $C_2 = 0.3$, whereas Hossain and Rodi [17] used $C_2 = 0.55$ for buoyant flows.

The buoyant part $\Phi_{ij}^{(3)}$ is difficult to study separately from the other pressure–strain contributions. For lack of sufficient experimental data, one usually models the buoyant part analogously to equation (4):

$$\Phi_{ij}^{(3)} = -C_3(G_{ij} - \tfrac{2}{3}G_k\delta_{ij}). \tag{5}$$

According to Launder [18], $C_3 = 0.33$ is an exact value in the case of isotropic turbulence. Gibson and Launder [19] took $C_3 = 0.5$ for the horizontal atmospheric boundary layer, Ljuboja and Rodi [20] used $C_3 = 0.6$ for horizontal and vertical natural-convection wall jets. To and Humphrey [5] used $C_3 = 0.55$ for the vertical natural-convection boundary layer, thus following Hossain and Rodi [17] and Gibson and Launder [21]. In general it seems best to take C_3 equal to C_2.

Although the three pressure–strain contributions are modeled separately, they will act simultaneously in most practical applications. Therefore the merits of the various modeling proposals should be judged from their performance in well-defined test cases. Gibson *et al.* [22] compared the performance of various sets of model constants reported in the literature. They found that the Quasi-Isotropic Model of Launder *et al.* [15] in combination with equations (2) and (5) is superior to the simple Rotta model (4), especially in non-equilibrium flows with strong anisotropy. For most practical applications, however, the simple Rotta model will give sufficient accuracy.

The diffusion term d_{ij} can be split into molecular diffusion (which is known exactly), turbulent diffusion involving a triple correlation, and pressure diffusion. Here, pressure diffusion is neglected, leaving only the triple correlation $\overline{u_i'u_j'u_k'}$ to be modeled. For $\overline{u_i'u_j'u_k'}$ a transport equation can be derived analogous to the Reynolds-stress equation (1), containing many new higher-order correlations which are difficult to model. Hanjalić and Launder [23] simplified the $\overline{u_i'u_j'u_k'}$ equation by dropping all transport terms and mean-flow contributions. Daly and Harlow [24] truncated that model as:

$$-\overline{u_i'u_j'u_k'} = C_s\frac{k}{\varepsilon}\overline{u_k'u_l'}\frac{\partial\overline{u_i'u_j'}}{\partial x_l} \tag{6}$$

where $C_s = 0.20$ [25], 0.22 [26] or 0.25 [15]. Although equation (6) is not invariant under coordinate rotation, it might still be an adequate model, if we assume that pressure diffusion is implicitly incorporated as well. The Daly and Harlow model can be generalized to the so-called gradient-diffusion model:

$$-\overline{u_i'\phi'} = C_\phi\frac{k}{\varepsilon}\overline{u_i'u_k'}\frac{\partial\Phi}{\partial x_k}. \tag{7}$$

Viscous dissipation of turbulence occurs at the smallest length scales, where turbulence is considered to be almost isotropic. This leads to an isotropic model for ε_{ij}:

$$\varepsilon_{ij} = \tfrac{2}{3}\varepsilon\delta_{ij}. \tag{8}$$

Lumley [14] stated that ε_{ij} can also contain off-diagonal terms, but these can be thought to be incorporated implicitly in the pressure–strain model. To close the Reynolds-stress model at this stage, we need additional equations for k, ε and $\overline{u_i'\theta'}$. The k equation follows directly from equation (1) under contraction of indices. For ε an exact transport equation can be derived, to be modeled with a second-moment closure. Following Tennekes and Lumley [27] we obtain:

$$U_k\frac{\partial\varepsilon}{\partial x_k} = \frac{\partial}{\partial x_k}\left(\nu\frac{\partial\varepsilon}{\partial x_k} + C_\varepsilon\frac{k}{\varepsilon}\overline{u_k'u_l'}\frac{\partial\varepsilon}{\partial x_l}\right) + C_{\varepsilon1}(P_k + C_{\varepsilon3}G_k)\frac{\varepsilon}{k} - C_{\varepsilon2}\frac{\varepsilon^2}{k}. \tag{9}$$

The values of the model constants $C_{\varepsilon1}$, $C_{\varepsilon2}$, $C_{\varepsilon3}$ are taken from the low-Reynolds-number k–ε model of Chien [3], whereas C_ε appears as a result of equation (7). One usually takes C_ε such that $C_\varepsilon/C_s = \sigma_k/\sigma_\varepsilon$, where σ_k and σ_ε are turbulent Prandtl numbers for k and ε in the k–ε model. Launder [25] recommended $C_s = 0.20$ and $C_\varepsilon = 0.15$, in accordance with $\sigma_k = 1.0$, $\sigma_\varepsilon = 1.3$. Hossain and Rodi [17] and To and Humphrey [5], however, took $C_s = 0.24$, which is not supported by experimental evidence.

2.2. *Modeling the turbulent heat flux equation*

The transport equation for the turbulent heat flux $\overline{u_i'\theta'}$ can be derived analogously to the Reynolds-stress equation (1):

$$U_k\frac{\partial\overline{u_i'\theta'}}{\partial x_k} = d_{i\theta} + P_{i\theta}^{(1)} + P_{i\theta}^{(2)} + G_{i\theta} + \Phi_{i\theta} - \varepsilon_{i\theta} \tag{10}$$

where

$$d_{i\theta} = \frac{\partial}{\partial x_k}\left(\nu\overline{u_i'\frac{\partial\theta'}{\partial x_k}} + \alpha\overline{\theta'\frac{\partial u_i'}{\partial x_k}} - \overline{u_i'u_k'\theta'} - \overline{\frac{p'\theta'}{\rho}}\delta_{ik}\right)$$

$$P_{i\theta}^{(1)} = -\overline{u_k'\theta'}\frac{\partial U_i}{\partial x_k};\quad P_{i\theta}^{(2)} = -\overline{u_i'u_k'}\frac{\partial\Theta}{\partial x_k};$$

$$G_{i\theta} = -g_i\beta\overline{\theta'^2};$$

$$\Phi_{i\theta} = \overline{\frac{p'}{\rho}\frac{\partial\theta'}{\partial x_i}};\quad \varepsilon_{i\theta} = (\nu+\alpha)\overline{\frac{\partial u_i'}{\partial x_k}\frac{\partial\theta'}{\partial x_k}}.$$

The terms on the right-hand side of equation (10) bear a close resemblance to the terms in equation (1). An important difference, however, is that $\overline{u_i'\theta'}$ is generated by both the mean-velocity gradient and the mean-temperature gradient. As a consequence of the Boussinesq approximation, buoyancy effects involve the temperature variance $\overline{\theta'^2}$, for which an additional relationship is needed.

For $\Phi_{i\theta}$ an integral expression can be obtained similar to the pressure–strain correlation, in which again four contributions can be distinguished: $\Phi_{i\theta}^{(1)}$, $\Phi_{i\theta}^{(2)}$, $\Phi_{i\theta}^{(3)}$, and a surface integral which is neglected far enough from fixed walls. For the turbulent part, Monin [28] proposed:

$$\Phi_{i\theta}^{(1)} = -C_{1\theta}\frac{\varepsilon}{k}\overline{u_i'\theta'} \tag{11}$$

followed by many workers. For $C_{1\theta}$ a value of about 3.0 is often used. Gibson and Launder [21] took $C_{1\theta} = 3.2$, but Wyngaard [29] used $C_{1\theta} = 4.8$. From the non-equilibrium data of Tavoularis and Corrsin [30], $C_{1\theta} = 3.7$ can be derived.

The mean-field part is usually modeled with the destruction-of-production hypothesis:

$$\Phi_{i\theta}^{(2)} = -C_{2\theta}P_{i\theta}^{(1)} \tag{12}$$

with $C_{2\theta} = 0.5$ according to most workers.

For the buoyant part one often uses, in analogy with equation (12):

$$\Phi_{i\theta}^{(3)} = C_{3\theta}g_i\beta\overline{\theta'^2} = -C_{3\theta}G_{i\theta}. \tag{13}$$

Launder [31] stated that $C_{3\theta} = 0.33$ is the correct value in the limit of vanishing anisotropy, but for most applications $C_{3\theta} = C_{2\theta} = 0.5$ will be a better choice.

In modeling the diffusion term $d_{i\theta}$, most authors neglected the pressure diffusion part, whereas others treated this term in combination with $\Phi_{i\theta}$. Here, we will neglect the pressure diffusion part. To obtain a simple expression for the molecular part, some terms have to be rewritten:

$$\frac{\partial}{\partial x_k}\left(\nu\overline{u_i'\frac{\partial\theta'}{\partial x_k}} + \alpha\overline{\theta'\frac{\partial u_i'}{\partial x_k}}\right) = \nu\frac{\partial^2\overline{u_i'\theta'}}{\partial x_k^2} + (\alpha-\nu)\overline{u_i'\frac{\partial^2\theta'}{\partial x_k^2}} + (\alpha-\nu)\overline{\frac{\partial u_i'}{\partial x_k}\frac{\partial\theta'}{\partial x_k}}. \tag{14}$$

The first term on the right-hand side of equation (14) is recognized as the desired molecular diffusion term, with ν as a diffusion coefficient. The second term on the right-hand side of equation (14) can be modeled with equation (7), yielding a third-order derivative in Θ, which is usually neglected. The last term in equation (14) can be modeled together with $\varepsilon_{i\theta}$. The above derivation, however, is not unique. In a similar way one can obtain a decomposition with α as a leading diffusion coefficient. Since it is not possible to decide a priori which choice will be best, we used the mean $(\alpha+\nu)/2$ as a diffusion coefficient. It is expected that this choice will only affect the viscous near-wall region of the flow. The last term which remains to be modeled is the triple correlation term $\overline{u_i'u_j'\theta'}$, representing turbulent diffusion. Wyngaard and Coté [32] used the generalized gradient-diffusion model (7) to find:

$$-\overline{u_i'u_j'\theta'} = C_\theta\frac{k}{\varepsilon}\overline{u_j'u_k'}\frac{\partial\overline{u_i'\theta'}}{\partial x_k} \tag{15}$$

with $C_\theta = 0.15$ [33] or $C_\theta = 0.20$ [25].

The viscous dissipation rate $\varepsilon_{i\theta}$ is the last term in the $\overline{u_i'\theta'}$ equation (10). At high turbulence Reynolds numbers, the small-scale turbulence is believed to be almost isotropic. A reversion of coordinate directions gives $x_k^* = -x_k$, $u_k^* = u_k$ and $\Theta^* = \Theta$. Assuming that $\varepsilon_{i\theta} = a$, we find $\varepsilon_{i\theta} = -a$ after reversion of coordinates. This is compatible only if $\varepsilon_{i\theta} = 0$. For this reason we will neglect $\varepsilon_{i\theta}$ altogether.

2.3. *Modeling the temperature variance equation*

For $\overline{\theta'^2}$ a differential equation similar to the k equation can be derived:

$$U_k\frac{\partial\overline{\theta'^2}}{\partial x_k} = d_\theta + 2P_\theta - 2\varepsilon_\theta \tag{16}$$

with

$$d_\theta = \frac{\partial}{\partial x_k}\left(\alpha\frac{\partial\overline{\theta'^2}}{\partial x_k} - \overline{u_k'\theta'^2}\right)$$

$$P_\theta = -\overline{u_k'\theta'}\frac{\partial\Theta}{\partial x_k}; \quad \varepsilon_\theta = \alpha\overline{\frac{\partial\theta'}{\partial x_k}\frac{\partial\theta'}{\partial x_k}}.$$

In this equation one can distinguish a diffusion term d_θ, a mean-flow production term P_θ and a thermal dissipation term ε_θ. The only correlations to be modeled are $\overline{u_k'\theta'^2}$ and ε_θ.

For the triple correlation, Samaraweera [34] used equation (7), where we will take $C_{\theta\theta} = 0.22$ as an appropriate model constant.

For ε_θ a transport equation can be derived. Jones and Musonge [35] started from the exact differential equation for ε_θ, which they modeled similarly to the ε equation in the standard KEM, the main difference being the use of two time scales instead of one:

$$U_k\frac{\partial\varepsilon_\theta}{\partial x_k} = \frac{\partial}{\partial x_k}\left(\alpha\frac{\partial\varepsilon_\theta}{\partial x_k} - \overline{u_k'\varepsilon_\theta'}\right) + \left(C_{P1}\frac{P_\theta}{\overline{\theta'^2}} - C_{D1}\frac{\varepsilon_\theta}{\overline{\theta'^2}}\right)\varepsilon_\theta + \left(C_{P2}\frac{P_k}{k} - C_{D2}\frac{\varepsilon}{k}\right)\varepsilon_\theta. \tag{17}$$

In modeling the turbulent diffusion term $\overline{u_k'\varepsilon_\theta'}$, the generalized gradient-diffusion model (7) is applied with $C_{\varepsilon\theta} = 0.22$, in accordance with Jones and Musonge [36]. For the model constants C_{P1}, C_{P2}, C_{D1} and C_{D2}, the set given by Nagano and Kim [37] is used: $C_{P1} = 1.8$, $C_{P2} = 0.72$, $C_{D1} = 2.2$, $C_{D2} = 0.8$.

In modeling the equations for $\overline{u_i'\theta'}$ and $\overline{\theta'^2}$, the mechanical turbulence time scale $\tau_m = k/\varepsilon$ has been used. Launder and Samaraweera [38] also considered the application of a thermal time scale $\tau_\theta = \frac{1}{2}\overline{\theta'^2}/\varepsilon_\theta$.

This leads to an overall time scale $\tau = \sqrt{(\tau_m \tau_\theta)}$, but since τ_θ is difficult to measure, most workers assume a linear relationship between both time scales, implying only one independent time scale. The ratio $R = \tau_\theta/\tau_m$ is usually assumed to lie between 0.5 and 1.0, but Jones and Musonge [35] used $R = 0.35$. Experiments have indicated that R is not a universal constant, but depends on the flow type. Béguier *et al.* [39] and Nagano and Hishida [40] observed $R \approx 0.4$–0.5 for the natural-convection boundary layer. With this simplification, we can put

$$\varepsilon_\theta = \frac{1}{2R}\overline{\theta'^2}\varepsilon/k.$$

If we assume that $\overline{\theta'^2}$ has only a small effect on the turbulent heat fluxes, we can assume local equilibrium $P_\theta = \varepsilon_\theta$, yielding:

$$\overline{\theta'^2} = -2R\frac{k}{\varepsilon}\overline{u_k'\theta'}\frac{\partial \Theta}{\partial x_k}. \tag{18}$$

This closes the set of Reynolds-stress equations.

3. BOUNDARY LAYER EQUATIONS

3.1. *Wall proximity and low-Reynolds-number effects*

Close to the wall the turbulence structure is strongly influenced by wall damping and pressure reflections, as shown in Table 1. The near-wall anisotropy increases; energy is transferred from $\overline{v'^2}$ to $\overline{u'^2}$, whereas $\overline{w'^2}$ remains virtually unaffected; the shear stress $\overline{u'v'}$ is diminished. Most pressure–strain models fail to give a proper description of these effects as a result of the neglect of the surface term in the integral expression for Φ_{ij}.

Shir [42] proposed a relatively simple wall model by adding a correction term to $\Phi_{ij}^{(1)}$. Gibson and Launder [19] extended the Shir model to the mean-strain part and the buoyant part:

$$\begin{aligned}\Phi_{ij,w} = {} & C_{1w}\frac{\varepsilon}{k}\left(\overline{u_k'u_i'}n_k n_l\delta_{ij} - \tfrac{3}{2}\overline{u_i'u_k'}n_k n_j\right.\\ & \left. - \tfrac{3}{2}\overline{u_j'u_k'}n_k n_i\right) f_w(l/y) + C_{2w}\left(\Phi_{kl}^{(2)}n_k n_l\delta_{ij} - \tfrac{3}{2}\Phi_{ik}^{(2)}n_k n_j\right.\\ & \left. - \tfrac{3}{2}\Phi_{jk}^{(2)}n_k n_i\right) f_w(l/y) + C_{3w}\left(\Phi_{kl}^{(3)}n_k n_l\delta_{ij} - \tfrac{3}{2}\Phi_{ik}^{(3)}n_k n_j\right.\\ & \left. - \tfrac{3}{2}\Phi_{jk}^{(3)}n_k n_i\right) f_w(l/y)\end{aligned} \tag{19}$$

where $n = (n_1, n_2, n_3)$ is the unit vector normal to the wall and y is the coordinate normal to the wall. A shortcoming of this model is that $\overline{u'^2}$ and $\overline{w'^2}$ are treated equally, which is not in agreement with experiments. Gibson and Launder [19] used $C_{1w} = 0.5$ and $C_{2w} = 0.3$, whereas To and Humphrey [5] applied $C_{1w} = 0.6$ and $C_{2w} = 0.3$. All authors took $C_{3w} = 0$ for lack of adequate experimental data. Launder *et al.* [15] suggested a different wall model in combination with their Quasi-Isotropic Model for Φ_{ij}.

Table 1. Comparison of experimental data on free-shear and near-wall flows

	$\overline{u'^2}/k$	$\overline{v'^2}/k$	$\overline{w'^2}/k$	$-\overline{u'v'}/k$
Free shear [41]	0.94	0.49	0.57	0.34
Near-wall flows [22]	1.19	0.25	0.56	0.24

For the turbulent heat fluxes observations similar to the Reynolds stresses can be made. According to Gibson and Launder [19], we have:

$$\Phi_{i\theta,w} = -\left(C_{1\theta w}\frac{\varepsilon}{k}\overline{u_k'\theta'} + C_{2\theta w}\Phi_{k\theta}^{(2)} + C_{3\theta w}\Phi_{k\theta}^{(3)}\right) \times n_k n_i f_w(l/y). \tag{20}$$

For the present geometry, these wall modifications only affect the $\overline{v'\theta'}$ equation. Most investigators took $C_{1\theta w} = 0.5$, $C_{2\theta w} = C_{3\theta w} = 0$.

In equations (19) and (20) f_w is a function decreasing with wall distance y. Gibson and Launder [19] took l to be the characteristic turbulence length scale $k^{3/2}/\varepsilon$, yielding

$$f_w(l/y) = \frac{k^{3/2}}{c_w \varepsilon y}. \tag{21}$$

For a forced-convection boundary layer f_w will be a monotonically decreasing function. It is not a priori clear whether the decrease in f_w also occurs for the natural-convection boundary layer. The value of the model constant c_w can be estimated from the wall functions for forced-convection flows: $c_w = \kappa/C_\mu^{3/4} \approx 2.5$ achieves $f_w = 1$ at the wall ($\kappa \approx 0.42$ Von Kármán constant). Ljuboja and Rodi [20] used a higher value $c_w = 3.72$ for buoyant flows. To and Humphrey [5] took $c_w = 2.53$ in their ASM calculations of the vertical natural-convection boundary layer.

In the highly anisotropic wall layer with the low turbulence levels, the assumption of small-scale isotropy for the viscous dissipation rate ε_{ij} is not valid. A correction term for ε_{ij} was suggested by Hanjalić and Launder [43]

$$\varepsilon_{ij} = \tfrac{2}{3}\varepsilon\left((1-f_s)\delta_{ij} + \tfrac{2}{3}f_s\frac{\overline{u_i'u_j'}}{k}\right) \tag{22}$$

with $f_s = (1 + Re_t/10)^{-1}$ and $Re_t = k^2/(\varepsilon\nu)$. In the outer region of the boundary layer f_s will be negligibly small.

Additional modifications are required to enforce a correct near-wall behavior of turbulence quantities. This is supported by a Taylor-series expansion for the basic fluctuating quantities in the vicinity of the wall, yielding $u' \sim y$, $v' \sim y^2$, $w' \sim y$ and $\theta' \sim y$. Chien [3] and Nagano and Kim [37] used these results to derive Taylor-series expansions for the turbulence quantities k, ε, $\overline{\theta'^2}$ and ε_θ. It follows that k and $\overline{\theta'^2}$ both behave as y^2 close to the wall, but ε and ε_θ both remain finite at the wall. For numerical convenience, however, ε and ε_θ are assumed to be isotropic, with $\varepsilon = \varepsilon_\theta = 0$ as wall boundary conditions. This necessitates the inclusion of the wall modification functions D and D_θ in the k and $\overline{\theta'^2}$ equations, which follows from an order-of-magnitude analysis for small y. Close to the

wall all terms in the k and $\overline{\theta'^2}$ equations vanish, except the molecular diffusion terms. Therefore, Jones and Launder [2] and Nagano and Kim [37] used correction terms of first-order accuracy in y. Chien [3] applied a somewhat simpler form for D with only zero order accuracy, but which proves to be sufficient for most computations. Therefore we will take

$$D = -2\nu\frac{k}{y^2}; \quad D_\theta = -2\alpha\frac{\overline{\theta'^2}}{y^2}. \tag{23}$$

To obtain wall-modification functions for the Reynolds-stress quantities, the dissipation ε_{ij} is approximated with a Taylor-series expansion around $y = 0$. Here, the anisotropy of the flow becomes apparent, since ε_{11} and ε_{33} remain finite at the wall, but $\varepsilon_{22} \sim y^2$ and $\varepsilon_{12} \sim y$ (see Launder and Reynolds [44]). From an order-of-magnitude analysis for the Reynolds-stress equations with y approaching zero, it is evident that wall modification functions D_{11}, D_{33} and D_{12} are required. Strictly speaking, a D_{22} function is not needed, since other terms in the $\overline{v'^2}$ equation ensure balance. Using a zero-order model equivalent to (23) yields

$$D_{11} = -2\nu\frac{\overline{u'^2}}{y^2}; \quad D_{22} = -8\nu\frac{\overline{v'^2}}{y^2};$$

$$D_{33} = -2\nu\frac{\overline{w'^2}}{y^2}; \quad D_{12} = -4\nu\frac{\overline{u'v'}}{y^2}. \tag{24}$$

These formulae are used in the PDEs for the Reynolds stresses. To achieve consistency with the k equation, we have put $D_{22} = -2\nu\overline{v'^2}/y^2$ so that $D_{ii} = 2D$.

For the turbulent heat fluxes the same argumentation is applied. For high Re_t the dissipation $\varepsilon_{i\theta}$ was modeled as zero. Close to the wall, however, the molecular diffusion terms have to be balanced by wall-modification functions. In accordance with Taylor-series expansions for the fluctuations, we find

$$D_{1\theta} = -(\nu+\alpha)\frac{\overline{u'\theta'}}{y^2}; \quad D_{2\theta} = -2(\nu+\alpha)\frac{\overline{v'\theta'}}{y^2}. \tag{25}$$

This completes the derivation of appropriate wall-modification functions. In the ε equation, additional low-Reynolds-number functions F_1, F_2 and E given by Chien [3] are included. Detailed information on low-Reynolds-number k–ε modeling is given by Patel *et al.* [45] and Henkes and Hoogendoorn [1]. For the ε_θ equation similar functions might be adequate, as was put forward by Nagano and Kim [37], but theoretical and experimental investigations are not yet available to determine suitable forms, so we will refrain from using them.

3.2. *Modeled equations*

3.2.1. *Fully differential Reynolds-stress model.* With the modeling approximations treated above, the partial differential equations in the RSM are simplified by a boundary-layer approximation. A complete description of the solved RSM equations is presented in Table 2, where

$$P_k = -\overline{u'v'}\frac{\partial U}{\partial y}, \quad G_k = g\beta\overline{u'\theta'},$$

$$P_\theta = -\overline{v'\theta'}\frac{\partial \Theta}{\partial y}, \quad C_{\varepsilon 3} = 1, \quad F_1 = 1,$$

$$F_2 = 1 - 0.3\exp(-Re_t^2/36)$$

and where we have omitted the convection and diffusion terms:

$$U\frac{\partial \phi}{\partial x} + V\frac{\partial \phi}{\partial y} = \Gamma_\phi\frac{\partial^2\phi}{\partial y^2} + C_\phi\frac{\partial}{\partial y}\left(\frac{k}{\varepsilon}\overline{v'^2}\frac{\partial \phi}{\partial y}\right) + \cdots.$$

The set is closed with the continuity equation (serving as the V equation) and the boundary-layer equations for U and Θ

$$\frac{\partial U}{\partial x} + \frac{\partial V}{\partial y} = 0 \tag{26}$$

$$U\frac{\partial U}{\partial x} + V\frac{\partial U}{\partial y} = \nu\frac{\partial^2 U}{\partial y^2} - \frac{\partial \overline{u'v'}}{\partial y} + g\beta(\Theta - \Theta_\infty) \tag{27}$$

$$U\frac{\partial \Theta}{\partial x} + V\frac{\partial \Theta}{\partial y} = \alpha\frac{\partial^2 \Theta}{\partial y^2} - \frac{\partial \overline{v'\theta'}}{\partial y}. \tag{28}$$

In our RSM, we have adopted the following models. For turbulent diffusion and pressure diffusion, the generalized gradient-diffusion hypothesis is used, since it is relatively simple and still accurate enough to capture most turbulent transport processes. More complicated models [23, 33] were implemented as well but gave no improvement of results. For the pressure–strain correlation we used the simple Rotta model. In the turbulent heat-flux equations the simple model of Monin [28] was used. In the ε_θ equation the model of Jones and Musonge [35] was used, in combination with the set of constants given by Nagano and Kim [37]. Wall modifications were modeled according to Gibson and Launder [19]. Furthermore, we added several low-Reynolds-number functions as described in the previous section.

3.2.2. *Algebraic Reynolds-stress model.* The PDEs for the Reynolds stresses, turbulent heat fluxes and temperature variance can be simplified to algebraic equations under the assumption of local equilibrium, thus dropping all transport terms. This approach may be justified for several types of free flow, but it is not realistic in the proximity of a solid wall. This is supported by the results of To and Humphrey [5], who showed that diffusion and convection terms in the k equation do not cancel close to the wall. As an improvement we applied the model of Rodi [46], who assumed a close analogy between transport of Reynolds stresses and transport of turbulent kinetic energy:

Table 2. Complete set of modeled Reynolds-stress equations

Variable	Mean-field production	Buoyant production	Viscous dissipation	Pressure–strain/scrambling			Near-wall modification
				Turbulent	Mean-strain	Buoyant	
k	P_k	G_k	$-\varepsilon$				$-2\nu\frac{k}{y^2}$
ε	$C_{\varepsilon 1}\frac{\varepsilon}{k}P_k$	$C_{\varepsilon 1}\frac{\varepsilon}{k}G_k$	$-C_{\varepsilon 2}F_2\frac{\varepsilon^2}{k}$				$-2\nu\frac{\varepsilon}{y^2}\exp(-0.5y^+)$
$\overline{u'v'}$	$-\overline{v'^2}\frac{\partial U}{\partial y}$	$g\beta\overline{v'\theta'}$	$-f_s\frac{\varepsilon}{k}\overline{u'v'}$	$-(C_1+\frac{3}{2}C_{1w}f_w)\frac{\varepsilon}{k}\overline{u'v'}$	$(1-\frac{3}{2}C_{2w}f_w)C_2\overline{v'^2}\frac{\partial U}{\partial y}$	$-C_3g\beta\overline{v'\theta'}$	$-4\nu\frac{\overline{u'v'}}{y^2}$
$\overline{u'\theta'}$	$-\overline{v'\theta'}\frac{\partial U}{\partial y}-\overline{u'v'}\frac{\partial\Theta}{\partial y}$	$g\beta\overline{\theta'^2}$		$-C_{1\theta}\frac{\varepsilon}{k}\overline{u'\theta'}$	$C_{2\theta}\overline{v'\theta'}\frac{\partial U}{\partial y}$	$-C_{3\theta}g\beta\overline{\theta'^2}$	$-(\nu+\alpha)\frac{\overline{u'\theta'}}{y^2}$
$\overline{v'\theta'}$	$-\overline{v'^2}\frac{\partial\Theta}{\partial y}$			$-(C_{1\theta}+C_{1\theta w}f_w)\frac{\varepsilon}{k}\overline{v'\theta'}$			$-2(\nu+\alpha)\frac{\overline{v'\theta'}}{y^2}$
$\overline{u'^2}$	$2P_k$	$2G_k$	$-\frac{2}{3}\varepsilon\left(1-f_s+\frac{3}{2}f_s\frac{\overline{u'^2}}{k}\right)$	$-C_1\varepsilon\left(\frac{\overline{u'^2}}{k}-\frac{2}{3}\right)+C_{1w}f_w\frac{\varepsilon}{k}\overline{v'^2}$	$-\frac{2}{3}C_2(2-C_{2w}f_w)P_k$	$-\frac{4}{3}C_3G_k$	$-2\nu\frac{\overline{u'^2}}{y^2}$
$\overline{v'^2}$			$-\frac{2}{3}\varepsilon\left(1-f_s+\frac{3}{2}f_s\frac{\overline{v'^2}}{k}\right)$	$-C_1\varepsilon\left(\frac{\overline{v'^2}}{k}-\frac{2}{3}\right)-2C_{1w}f_w\frac{\varepsilon}{k}\overline{v'^2}$	$\frac{2}{3}C_2(1-2C_{2w}f_w)P_k$	$\frac{2}{3}C_3G_k$	$-2\nu\frac{\overline{v'^2}}{y^2}$
$\overline{w'^2}$			$-\frac{2}{3}\varepsilon\left(1-f_s+\frac{3}{2}f_s\frac{\overline{w'^2}}{k}\right)$	$-C_1\varepsilon\left(\frac{\overline{w'^2}}{k}-\frac{2}{3}\right)+C_{1w}f_w\frac{\varepsilon}{k}\overline{v'^2}$	$\frac{2}{3}C_2(1+C_{2w}f_w)P_k$	$\frac{2}{3}C_3G_k$	$-2\nu\frac{\overline{w'^2}}{y^2}$
$\overline{\theta'^2}$	$2P_\theta$		$-2\varepsilon_\theta$				$-2\alpha\frac{\overline{\theta'^2}}{y^2}$
ε_θ	$C_{P1}\frac{P_\theta}{\overline{\theta'^2}}\varepsilon_\theta+C_{P2}\frac{P_k}{k}\varepsilon_\theta$		$-C_{D1}\frac{\varepsilon_\theta}{\overline{\theta'^2}}\varepsilon_\theta-C_{D2}\frac{\varepsilon}{k}\varepsilon_\theta$				

$$\frac{\mathrm{D}\overline{u_i'u_j'}}{\mathrm{D}t} - d_{ij} \approx \frac{\overline{u_i'u_j'}}{k}\left(\frac{\mathrm{D}k}{\mathrm{D}t} - d_k\right)$$

$$= \frac{\overline{u_i'u_j'}}{k}(P_k + G_k - \varepsilon) \quad (29)$$

where $d_k = \frac{1}{2}d_{ii}$ represents diffusion of k. This approximation seems particularly useful for the normal stresses, but is not a priori correct for the shear stresses, as was argued by Hossain and Rodi [17]. Therefore we used equation (29) for the normal stresses only. Gibson and Launder [19] extended Rodi's idea to the turbulent heat fluxes, but their formulation has not been widely tested and seems somewhat questionable from a theoretical point of view.

3.3. *Boundary conditions*

In general, for each partial differential equation one boundary condition is required in the x-direction and two boundary conditions are needed in the y-direction. No boundary conditions are specified at the downstream edge $x = x_\infty$, since the PDEs are parabolic in the x-direction. In Fig. 1 the computational domain is depicted together with boundary conditions.

At $x = x_b$ an initial flow field is imposed. Two different options are used: a laminar and a turbulent starting profile. The laminar profile is calculated from the similarity solution of Ostrach [47]. In this case, the transition from laminar to turbulent flow has to be triggered by introducing a small amount of turbulent kinetic energy at a certain point in the flow, characterized by $Gr_x = Gr_{tr}$. From experiments a Gr_{tr}-value of about 2×10^9 seems to be reasonable. The k-level at the transition line is set equal to $k/u_b^2 \approx 4 \times 10^{-4}$, with $u_b = \sqrt{(g\beta\Delta\Theta x)}$. The corresponding ε-profile is calculated from a local equilibrium assumption, yielding

$$\varepsilon = \sqrt{C_\mu}k\left|\frac{\partial u}{\partial y}\right|.$$

Furthermore, prescribing non-homogeneous Dirichlet conditions at the outer edge for k and ε enhances the transition. Characteristically, k and ε are chosen such that $Re_t \approx 75$ at the outer edge.

The turbulent starting profile is applied at $x = x_b$,

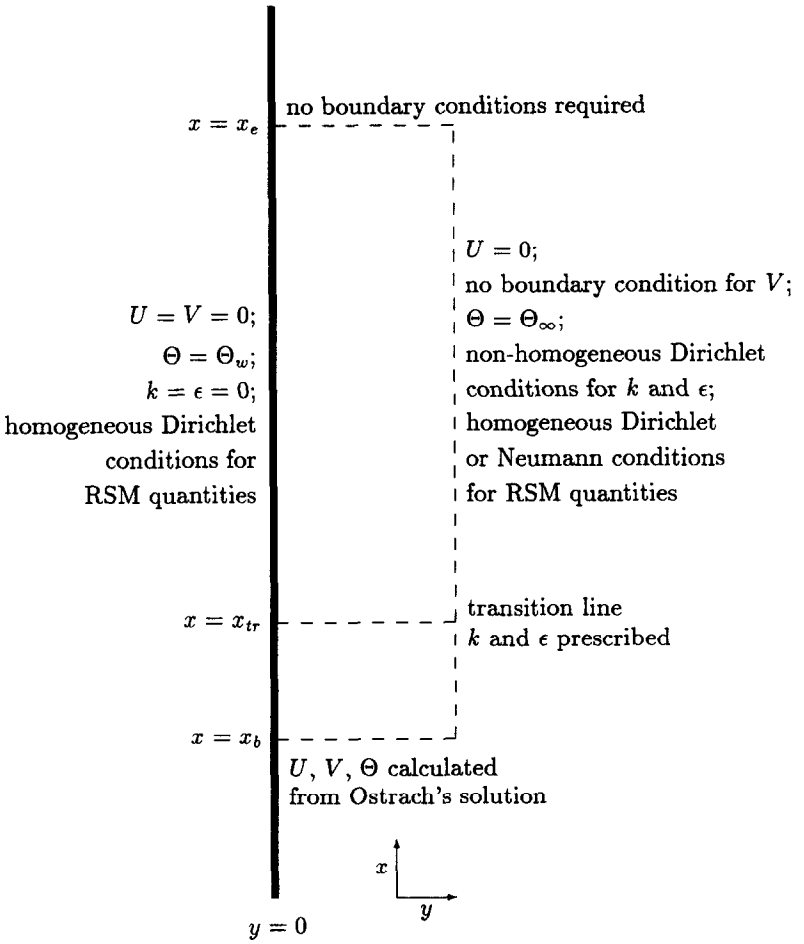

FIG. 1. Geometry, computational domain and boundary conditions.

by using experimental correlations for the turbulent wall-heat transfer and by assuming the similarity relationships of George and Capp [48]. Our computations show that the numerical solution immediately falls back to the laminar branch for $Gr_x < Gr_{tr}$. For larger Gr_x, the solution finally becomes fully turbulent. Therefore, for smaller Gr_x there seems to exist only a laminar solution, but for $Gr_x > Gr_{tr}$ instabilities can arise, which cause the transition from the laminar to the turbulent flow. In some cases the flow field remains laminar up to very large Gr_x-values. Increasing the amount of introduced turbulent kinetic energy at the transition station and at the outer edge gives a quicker transition.

In the asymptotic limit of large Gr_x the boundary-layer structure turns out to be independent of the choice of boundary conditions for k and ε and of the applied starting profile; the exact nature and location of the transition process is considered to be of minor importance.

4. NUMERICAL METHOD

The partial differential equations in the KEM, ASM and RSM were discretized with a control-volume method. In general, the control-volume method is applied to elliptic flow problems. Here we used a modified version, which incorporates the parabolic character of boundary-layer flows. The present boundary-layer code was originally developed in ref. [1]. For this study, Reynolds-stress model equations were implemented.

Rectangular grid cells are used to avoid cross derivatives in calculating the fluxes through the cell boundaries. A disadvantage is that the outer edge of the computational domain does not closely follow the boundary-layer edge for small x-values. Especially in the laminar part of the flow this leads to a considerable amount of ineffective grid cells. In the x-direction a uniform grid is used. In the y-direction a non-uniform grid is adopted, locating more grid cells close to the wall where gradients are steepest. This has two advantages: wall gradients are calculated more accurately, and more grid cells fall in the inner part of the boundary layer, thus reducing the number of ineffective grid cells. A tangens hyperbolicus formula is used to generate the y-grid.

Having established a suitable computational grid, the various convection and diffusion terms were discretized. In the boundary-layer approximation x-diffusion is neglected, leaving only x-convection to be discretized, which was done by a first-order upwind scheme. In the y-direction we adopted a hybrid scheme, which switches from central to upwind discretization, depending on the local mesh Péclet number. A numerical solution was obtained with a line-by-line Gauß–Seidel iteration method, using the tridiagonal matrix algorithm. To aid numerical stability, the grid was staggered in the y-direction for the V-velocity and all Reynolds-stress quantities. In the x-direction no staggering was required.

Special attention has to be paid to the boundary conditions at the wall and at the outer edge. For the V-velocity, with grid points coinciding with the wall and the outer edge, no problems arise, since we can simply specify $V = 0$ at the wall. No boundary condition is required at the outer edge for the V equation, since it is of first order. For the Reynolds-stress quantities, the wall boundary conditions are treated analogously to the V-velocity, since they are calculated on the same staggered y-grid. At the outer edge, we can specify either homogeneous Neumann boundary conditions or Dirichlet conditions. Since the grid points for U, Θ, k and ε do not coincide with the wall or the outer edge, virtual grid points are needed to discretize the boundary conditions.

Iacovides and Launder [49], who solved ASM equations for complicated flows, encountered several obstacles in obtaining a converged numerical solution. From their suggestions we adopted the ones relevant to our case. In short, we modified our solution method as follows: staggering of Reynolds stresses; introduction of pseudo-viscosities; modification of source terms in the k–ε equations; iterative solution method for algebraic Reynolds-stress equations. For further details, see ref. [49].

As a convergence criterion, we demanded that in all grid points all variables, non-dimensionalized such that their maximum absolute values are of order unity, should vary less than 10^{-4} between two successive iterations. A sharper criterion did not improve the results. To prevent the numerical solution process from oscillating or diverging, we used three methods: underrelaxation, false time steps and source-term manipulation (which treats positive source terms explicitly and negative source terms implicitly). The exact values of the relaxation parameters and false time steps are not given here, since they largely depend on the solution method, the grid structure and the boundary conditions. Quick convergence could be obtained with about 100 iterations per line in the fully turbulent part of the boundary layer. In the transition region more iterations were required.

5. RESULTS AND DISCUSSION

5.1. *Literature review*

5.1.1. *Experimental data.* In the literature, not many experimental data exist on Reynolds-stress problems in the natural-convection boundary layer along a heated, vertical plate. Indeed, accurate measurements are difficult, due to the small thickness of the boundary layer and the limited accuracy of measuring instruments. The two most frequently used measuring techniques are hot-wire anemometry and laser–Doppler anemometry. The use of the hot-wire method has the disadvantage that the probe—although very small—forms an obstruction and dis-

torts the flow field. Tsuji and Nagano [7–9], however, claim that their recent hot-wire measurements are somewhat more accurate than existing laser–Doppler measurements.

The case of a semi-infinite plate in an isothermal environment can never be simulated exactly in a real laboratory situation. The box used by Tsuji and Nagano was much larger than other configurations reported in the literature, thus reducing temperature stratification at the outer edge of the boundary layer. Their measurements were conducted in air for uniform wall temperature, in contrast with Miyamoto *et al.* [6] who applied uniform wall-heat flux. Since the wall-heat transfer for large Gr_x behaves almost analogously for these two heating mechanisms, both experiments are used to verify the present calculations.

Tsuji and Nagano non-dimensionalized their turbulence quantities with u_τ and Θ_τ (suggesting an analogy with the forced-convection boundary layer), whereas Miyamoto *et al.* used $u_{\max}$ and $\Delta\Theta$. Here we will adopt the latter reference quantities. In general, the results of both investigations agree well for the outer part of the boundary layer. In the inner layer some differences appear. There, Miyamoto *et al.* observed $\overline{u'v'}$, $\overline{u'\theta'} < 0$ whereas Tsuji and Nagano found $\overline{u'v'}$, $\overline{u'\theta'} \approx 0$. Also the near-wall behavior of $\overline{v'^2}$ does not match.

5.1.2. *Numerical data.* Most Reynolds-stress models have been tuned for free shear flows. Only few authors also included buoyancy effects and wall influences, since an accurate description of these phenomena requires the introduction of additional model functions and constants which are very difficult to extract from the available experimental data.

The horizontal boundary layer was studied theoretically by Launder [18] and Gibson and Launder [19, 21]. The latter authors adopted the Shir-like wall modifications, whereas Launder [18] used the wall model of Launder *et al.* [15]. Gibson and Leslie [50] investigated the vertical boundary layer with an ASM. They mentioned some important limitations of their analysis. The assumption of local equilibrium seems invalid in the turbulent natural-convection boundary layer, which implies that a differential RSM should be used. Furthermore, it seems doubtful whether $f_w = f(l/y)$ is a correct wall modification function. Gibson and Leslie did not specify f_w explicitly, but assumed that f_w decreases monotonically from unity at the wall to zero in the outer layer.

Recently, To and Humphrey [5] carried out ASM calculations for the vertical boundary layer. Although their results are the best available, they found only qualitative agreement with measurements of Cheesewright and Ierokipiotis [51] and Miyamoto *et al.* [6]. Some of the differences are inherent to the ASM, but others stem from less complete modeling. Important for the whole turbulence structure is the calculation of the normal stresses. In general the lateral normal stress $\overline{v'^2}$ is more important than the other two normal stresses, since in the boundary-layer approximation $\overline{v'^2}$ appears in the generalized gradient-diffusion model (7) and in the production terms for $\overline{u'v'}$ and $\overline{v'\theta'}$. In the natural-convection boundary layer, the local-equilibrium assumption leads to an overestimation of all normal stresses, since $P_k + G_k > \varepsilon$ in most parts of the flow. To and Humphrey did not use an algebraic $\overline{w'^2}$ equation, but directly computed $\overline{w'^2} = 2k - \overline{u'^2} - \overline{v'^2}$. Hence, they computed too high levels for $\overline{u'^2}$ and $\overline{v'^2}$, and a too low $\overline{w'^2}$ level. An alternative is to calculate all three normal stresses by algebraic equations, and then scaling them in such a way that their sum equals $2k$. In this way consistency is achieved without overpredicting $\overline{u'^2}$ and $\overline{v'^2}$ strongly. A second, more sophisticated option is to model the transport of normal stresses according to Rodi [46]. In RSM calculations this problem is avoided, but due to small numerical errors it is still recommended to enforce consistency between the k-level and the normal stresses.

5.2. *Sensitivity analysis of RSM constants*

The influence of RSM constants on the computed mean-flow and turbulence structure cannot be derived easily from the set of RSM equations, since these are strongly coupled and non-linear. Therefore, a sensitivity analysis was carried out. The sensitivity parameter $S(\phi, \beta)$ is defined as a dimensionless measure for the sensitivity of a quantity ϕ to a change in model constant β, by taking $S(\phi, \beta) = (\beta/\phi)(\partial\phi/\partial\beta)$. For example, a value of $S = 0.1$ implies that a 1% increase in β will yield a 0.1% increase in ϕ.

We investigated $Nu_x = -x/\Delta\Theta(\partial\Theta/\partial y)_w$ and all mean-flow and turbulence variables, of which we considered the maximum values and their positions, all at $Gr_x = 10^{11}$ where the flow has become fully turbulent. These quantities were non-dimensionalized with x, $u_{\max}$ and $\Delta\Theta$, allowing us to compare them with experimental data. We made sure that our numerical results were sufficiently accurate and grid independent. For all calculations a laminar starting profile was applied. As a reference test, we took the set of model constants listed in Table 3. In each test we varied only one constant. The sensitivity results were obtained for RSM calculations, but qualitatively also apply to ASM calculations. Only the most important results are discussed here. Figure 2 shows the sensitivity of Nu_x, $u_{\max}$ and $k_{\max}/u^2_{\max}$. These three quantities are characteristic for the prediction of the inner layer, the mean velocity and the outer-layer turbulence. It is seen that the velocity maximum is almost insensitive to changes in model constants, whereas Nu_x and $k_{\max}$ are moderately sensitive to changes in most model constants.

The most influential RSM constants are C_1, $C_{1\theta}$, C_{1w} and c_w. Of slightly less importance are $C_{1\theta w}$, C_{2w} and C_s, whereas $C_{\theta\theta}$ and $C_{\varepsilon\theta}$ mainly affect ε_θ, $\overline{\theta'^2}$ and $\overline{u'\theta'}$. The constants C_{P1}, C_{P2}, C_{D1} and C_{D2} appearing in the ε_θ equation have a strong effect on $\overline{\theta'^2}$ and $\overline{u'\theta'}$, but have less influence on the main turbulence structure. The remaining model constants are not very

Table 3. Initial set of RSM and KEM constants

C_1	C_2	C_3	C_{10}	C_{20}	C_{30}	C_{1w}	C_{2w}	C_{10w}	c_w	C_s	C_ε	C_θ	$C_{\theta\theta}$	$C_{\varepsilon\theta}$	C_{P1}	C_{P2}	C_{D1}	C_{D2}	C_μ	$C_{\varepsilon 1}$	$C_{\varepsilon 2}$
2.2	0.55	0.55	3.75	0.5	0.5	0.6	0.3	0.75	2.53	0.20	0.15	0.20	0.22	0.22	1.8	0.72	2.2	0.8	0.09	1.35	1.80

important for the overall flow, and they control one or two specific quantities.

The modeling of the pressure–strain correlation and the pressure–temperature gradient correlation is essential in Reynolds-stress modeling. Since it is expected that in high turbulence levels the turbulent parts of these correlations will be dominant, it is not surprising that C_1 and $C_{1\theta}$ are found to be important. The fact that C_{1w} and c_w are also important is an indication of the significance of the wall-correction terms involving the f_w function.

The model constants appearing in the ε_θ equation dominate the behavior of temperature fluctuations. C_{P1} and C_{D1} are more important than C_{P2} and C_{D2}, indicating that the production and destruction of temperature fluctuations is mainly determined by the thermal quantities P_θ and ε_θ. Although further research is needed to tune these model constants more accurately, the set of constants given by Nagano and Kim [37] proved to be satisfactory for our calculations.

5.3. *Comparison with experiments*

5.3.1. *Heat transfer and mean-flow predictions.* Considering the various ranges of model constants reported in the literature, we see $1.5 < C_1 < 3.0$ and $3.0 < C_{1\theta} < 5.0$, whereas C_2 and $C_{2\theta}$ vary considerably as well. Within these ranges, local heat-transfer results vary strongly ($450 < Nu_x < 900$ at $Gr_x = 10^{11}$), but the velocity maximum is almost unchanged. Thus it is possible to tune the set of constants such that good agreement between numerical predictions and experiments can be obtained, without exceeding the range of literature values. Therefore, we chose $C_{1\theta} = 3.75$ and $C_{1\theta w} = 0.75$, to improve wall-heat transfer predictions for both ASM and RSM calculations. From the sensitivity analysis we decided to use our initial set listed in Table 3, with which good mean-flow results were obtained. It is stressed, however, that we did not adapt our set of constants to improve results on turbulence quantities. Before turning to the detailed turbulence structure, it is important to certify that our ASM and RSM calculations agree well with experimental mean-flow data.

In Figs. 3(a)–(c) the transition from laminar to turbulent flow can be clearly distinguished. In Fig. 3(a) the wall-heat transfer Nu_x is compared with the experimental data of Tsuji and Nagano [9], who found a $Gr_x^{1/3}$ dependence. Taking into account experimental inaccuracies, we see that KEM, ASM and RSM predictions all agree well with the experimental data. Figures 3(b) and (c) show two other important mean-flow parameters: u_{max}/u_b and $v_{t,max}/(xu_{max})$. These figures illustrate that at $Gr_x = 10^{11}$ the numerical solution has approached its asymptotic turbulent branch. It is seen that the maximum velocity predictions are in good agreement with the measurements of Tsuji and Nagano. The turbulent viscosity was calculated as $C_\mu F_\mu k^2/\varepsilon$.

Mean-velocity and mean-temperature profiles are

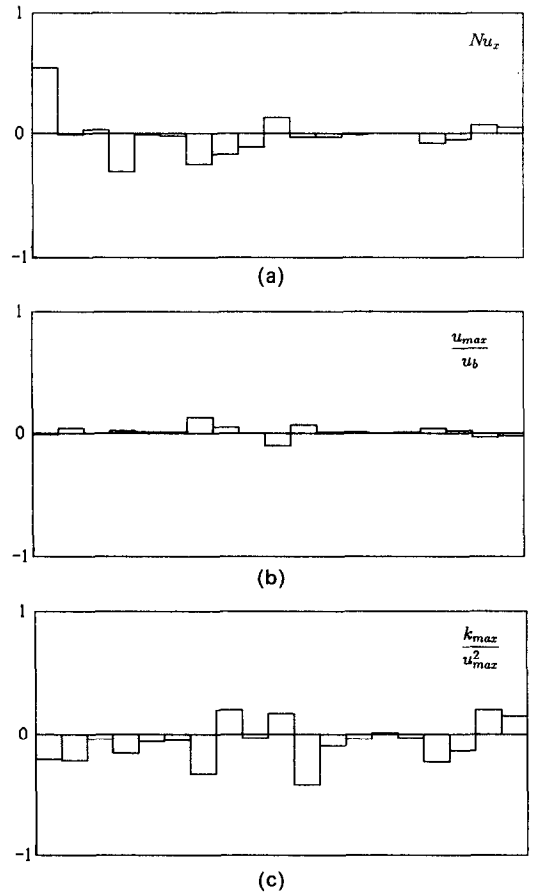

FIG. 2. Sensitivity analysis for several flow quantities. (a) Wall-heat transfer. (b) Velocity maximum. (c) Turbulent kinetic energy maximum. Plotted from left to right are C_1, C_2, C_3, $C_{1\theta}$, $C_{2\theta}$, $C_{3\theta}$, C_{1w}, C_{2w} $C_{1\theta w}$, c_w, C_s, C_ε, C_θ, $C_{\theta\theta}$, $C_{\varepsilon\theta}$, C_{P1}, C_{P2}, C_{D1} and C_{D2}.

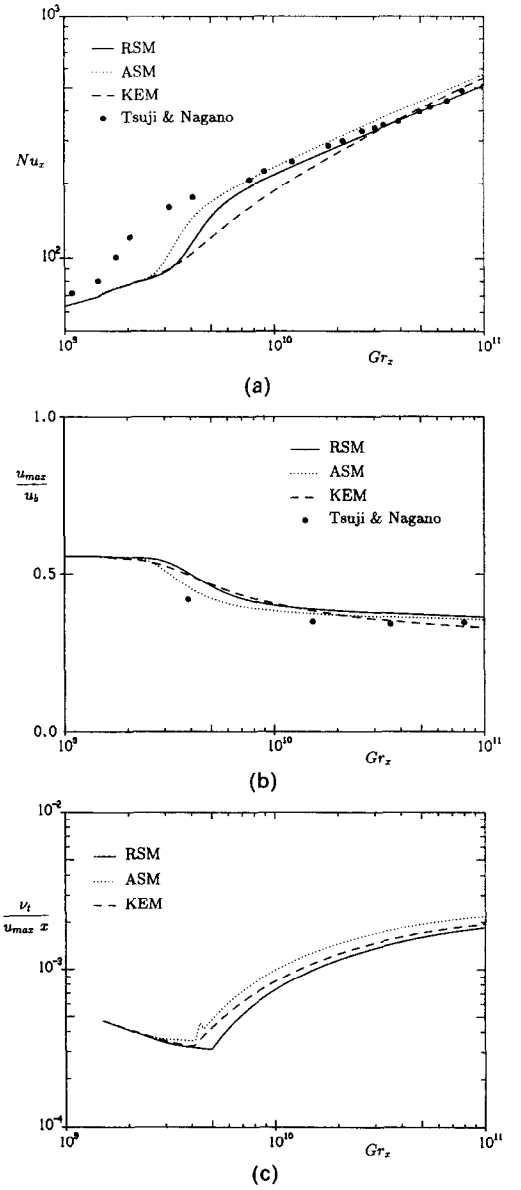

FIG. 3. Transition from laminar to turbulent flow. (a) Wall-heat transfer. (b) Velocity maximum. (c) Turbulent viscosity maximum.

depicted in Fig. 4, showing excellent agreement with experiments for all three models. In the outer part of the thermal boundary layer some differences are observed, which are probably due to a small temperature stratification in the experimental configuration. Hence, we conclude that our ASM and RSM are sufficiently accurate for mean-flow computations.

5.3.2. *Turbulence quantities.* Here, we will discuss turbulence characteristics at $Gr_x = 10^{11}$, where experimental data are depicted as symbols and numerical data by (dashed) lines. For the data of Tsuji and Nagano [7–9] we used circles (●); for the data of Miyamoto *et al.* [6] we used triangles (▲).

In Fig. 5, the calculated normal stresses are compared with the isotropic normal stress $\frac{2}{3}k$ derived from the KEM and RSM results. The ASM results (not plotted) exhibit approximately the same behavior as the RSM results. The KEM and RSM produce about the same k-profile, but the turbulence structure is highly anisotropic, in agreement with experiments. In accordance with theory and experiments, we find $\overline{v'^2} < \overline{w'^2} < \overline{u'^2}$ throughout the boundary layer, which is a markedly better result than that of To and Humphrey [5].

The normal stresses $\overline{u'^2}$ and $\overline{v'^2}$ are investigated further in Figs. 6(a) and (b). Since we enforced consistency with the computed turbulent kinetic energy by scaling the normal stresses such that their sum equals $2k$, the observed differences between ASM and RSM predictions are not very large. The calculated stress levels agree well with experiments. In the inner layer the data of Tsuji and Nagano for $\overline{v'^2}$ are followed better than those of Miyamoto *et al.* Possibly, this is a consequence of the wall-correction function D_{22} used in the $\overline{v'^2}$ equation. Taking the coefficient 8 instead of 2 in D_{22} will give a lower $\overline{v'^2}$ level in the inner layer, but consistency with the k equation will

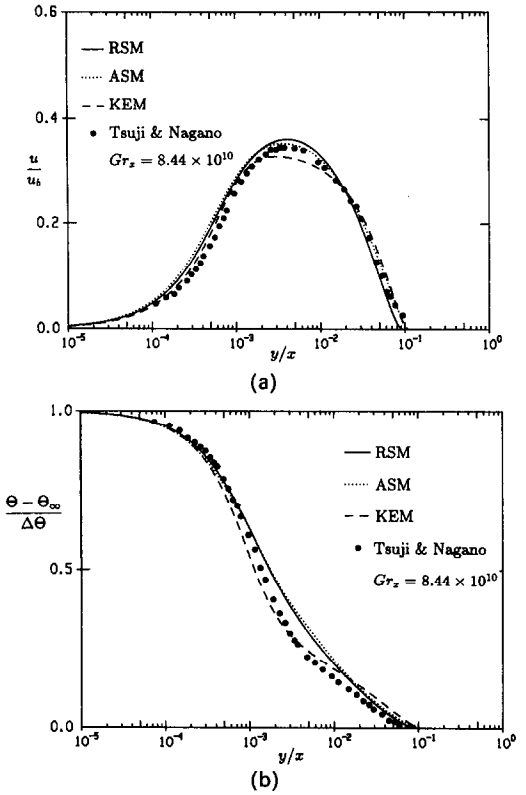

FIG. 4. Calculated mean velocity (a) and mean temperature profile (b) compared with experiments.

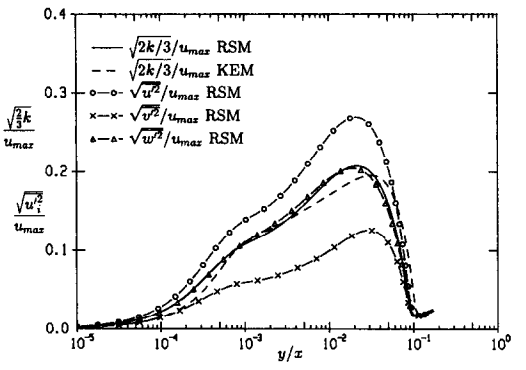

FIG. 5. R.m.s. velocity fluctuations from RSM compared with isotropic velocity fluctuations derived from KEM and RSM.

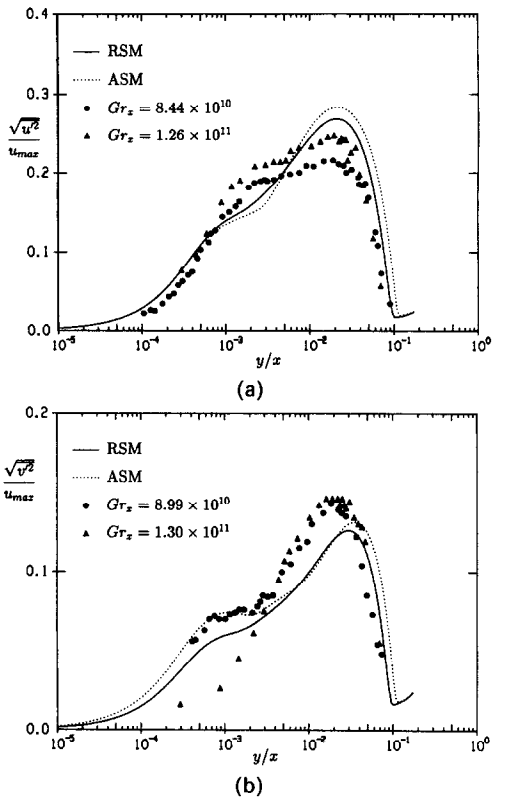

FIG. 6. Computed streamwise normal stress (a) and lateral normal stress (b) compared with experimental data.

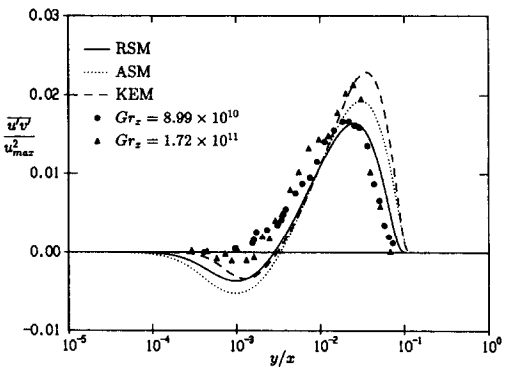

FIG. 7. Calculated Reynolds-shear stress compared with shear stress derived from KEM and experimental data.

no longer be exactly satisfied. Moreover, it is observed that in the outer layer $\overline{u'^2}$ is slightly overpredicted and $\overline{v'^2}$ is underpredicted. Increasing C_1 will give improvements on this point, but it will also affect other mean-flow and turbulence quantities. A second possibility is to use the Quasi-Isotropic Model of Launder *et al.* [15], which gives a somewhat better description of anisotropic turbulence. Our sensitivity analysis showed that $\overline{v'^2}_{max}$ is mainly sensitive to changes in C_1, C_{1w} and c_w, indicating that the wall model is of importance when predicting normal-stress levels even in the outer layer.

In Fig. 7 the shear stress $\overline{u'v'}$ is plotted, where we also included KEM results by taking $\overline{u'v'} = -\nu_t \partial U/\partial y$. The RSM predictions exhibit good overall agreement with experiments. In the outer layer the KEM gives a too high $\overline{u'v'}$; in the inner layer ASM results differ somewhat from measurements. All three models yield $\overline{u'v'} < 0$ in the inner layer. For the KEM no qualitative improvements seem possible, but ASM and RSM results may benefit from a different wall model for the surface term in Φ_{ij}. The wall model of Launder *et al.* [15] might provide an interesting alternative.

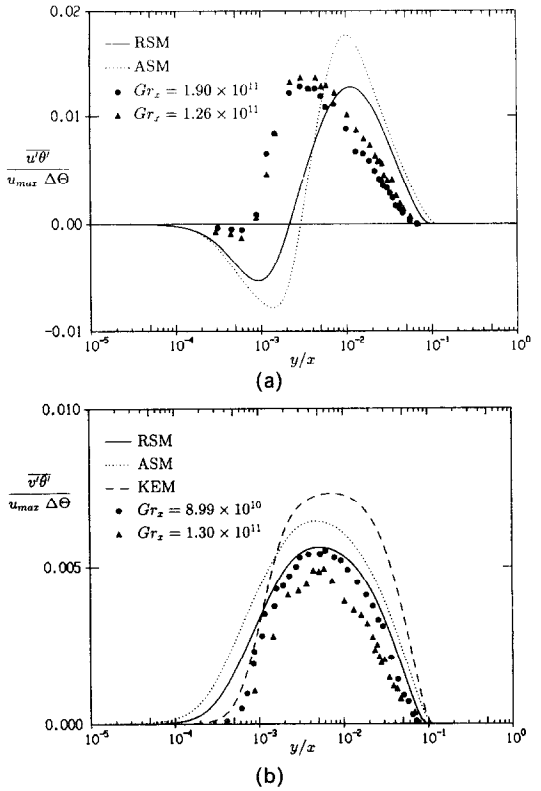

FIG. 8. Computed streamwise (a) and lateral (b) turbulent heat flux compared with measurements.

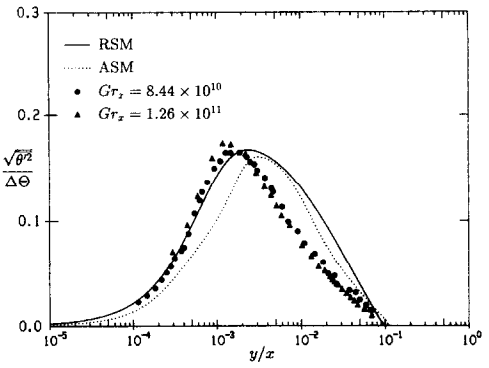

FIG. 9. Calculated temperature fluctuations compared with experiments.

In Fig. 8 the streamwise and lateral turbulent heat fluxes $\overline{u'\theta'}$ and $\overline{v'\theta'}$ are investigated for KEM, ASM and RSM, clearly showing the superiority of RSM predictions. The predicted $\overline{u'\theta'}$-profile is only in qualitative agreement with experiments, but RSM results are better than ASM results. The position of $\overline{u'\theta'}_{max}$ is shifted too far to the outer edge, and in the inner layer $\overline{u'\theta'} < 0$ is found in contradiction with experiments. In general the profiles for $\overline{u'\theta'}$ and $\overline{u'v'}$ show some similarity. A better inner layer prediction of $\overline{u'v'}$ might therefore also improve $\overline{u'\theta'}$ results. Furthermore, the use of a different wall model for $\Phi_{i\theta}$ seems to be required. The employed wall model (20) only affects the $\overline{v'\theta'}$ equation, but it seems realistic that $\overline{u'\theta'}$ is influenced by wall effects too. The wall model of Launder and Samaraweera [38] could serve as a better alternative here. The lateral turbulent heat flux $\overline{v'\theta'}$ is predicted very well by the RSM. ASM and KEM agree well qualitatively, but give a too high maximum value.

The temperature fluctuations $\overline{\theta'^2}$ are shown in Fig. 9. The RSM data agree well with experiments, especially in the inner layer. In the outer layer $\overline{\theta'^2}$ is overpredicted by both the ASM and the RSM. This might be due to the experimental temperature profiles, which were obtained in a slightly stratified medium. Also, improvements can be expected from a better model for the ε_θ equation. For the timescale ratio R we used $R = 0.35$ in the ASM, in close agreement with numerical data of Nagano and Kim [37] for the forced-convection boundary layer. RSM calculations showed, however, that R is not a constant over the flow. In the inner layer R reaches a maximum of about 0.7, but in the outer layer R remains virtually constant with $R \approx 0.3$. These results largely depend on the wall-modification functions in the k–ε equations (affecting τ_m) and the $\overline{\theta'^2}$–ε_θ equations (affecting τ_θ), especially in the near-wall region.

The theoretical near-wall y-dependence of the turbulence quantities, as derived with Taylor-series expansions, could be reproduced very well. We checked that this was a result of the inclusion of the correction terms D_{ij}, $D_{i\theta}$ and D_θ which account for anisotropic viscous dissipation. The shape of the f_w-function is related to the near-wall behavior. In forced convection this function decreases from unity to zero as y increases. Here, we found much higher values, with $f_w \approx 3$ in the inner layer. In the outer layer f_w is smaller but remains larger than 0.05. Although this is not the expected behavior, the f_w-function yields good predictions of the turbulence structure.

5.3.3. *Eddy-viscosity concept.* The eddy-viscosity concept is used in many lower-order closure models, assuming that turbulent transport of a quantity ϕ is related to its mean-flow gradient:

$$\overline{u_i'\phi'} = -\frac{\nu_t}{\sigma_\phi}\left(\frac{\partial \Phi}{\partial x_i}\right).$$

Our ASM and RSM calculations allow a check on the validity of this assumption in the natural-convection boundary layer.

The assumed isotropic turbulence structure in the eddy-viscosity concept is not reproduced by experiments and RSM calculations. This is illustrated by Figs. 5 and 6. In the outer layer, $\overline{u'v'}$ and $\overline{u'\theta'}$ are approximated reasonably well by the eddy-viscosity concept. In Fig. 10 we have depicted the eddy-viscosity for momentum $(-\overline{u'v'}/(\partial U/\partial y))$ and temperature $(-\overline{v'\theta'}/(\partial \Theta/\partial y))$, as derived from ASM and RSM results. They are compared with KEM results and data of Tsuji and Nagano. At the velocity maximum the eddy-viscosity for momentum shows a singularity, which is reproduced correctly by the ASM and the

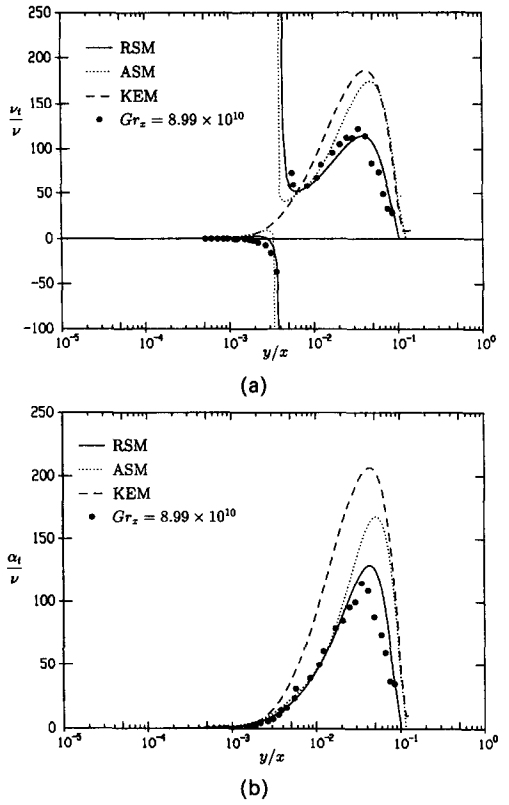

FIG. 10. Eddy-viscosity for velocity (a) and temperature (b) derived from ASM and RSM results, compared with KEM and experiments of Tsuji and Nagano.

RSM. The momentum-eddy-viscosity predicted by the RSM falls some 40% lower than KEM and ASM results, and agrees with the experimental data. The same observation holds for the temperature-eddy-viscosity. The ratio of these two eddy-viscosities is the turbulent Prandtl number σ_θ. From Fig. 11 we see that σ_θ exhibits the same singularity as ν_t, which is reproduced by the ASM and the RSM. In the inner layer the ASM and RSM results suggest $\sigma_\theta = 0.75$, but Tsuji and Nagano found $\overline{u'v'} \approx 0$ yielding $\sigma_\theta \approx 0$. In the outer layer the experiments and numerical results agree very well. In general, the assumption

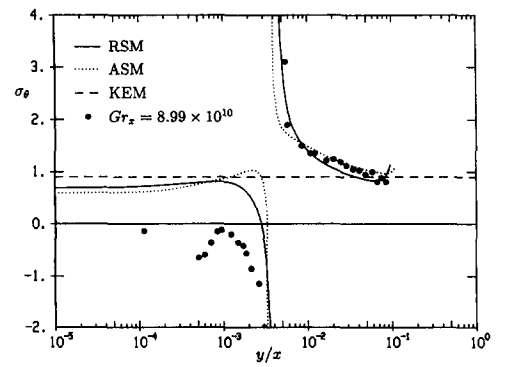

FIG. 11. Turbulent Prandtl number derived from ASM and RSM results, compared with KEM assumption and measurements of Tsuji and Nagano.

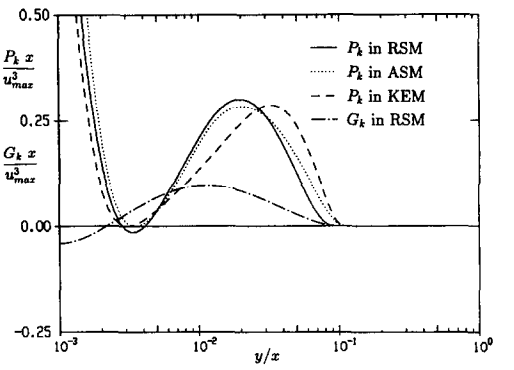

FIG. 12. Buoyant production G_k of turbulent kinetic energy in RSM, compared with shearing production P_k in RSM, ASM and KEM.

$\sigma_\theta = 0.9$ in the KEM seems reasonable, especially in the outer layer where turbulent diffusion is most prominent. In the inner layer, including the velocity maximum, σ_θ is certainly not a constant, but this does not affect mean-flow predictions very much.

Another important assumption of the eddy-viscosity concept is that turbulent transport occurs only in the direction of the mean gradient. Experimental and numerical data clearly reveal that $\overline{u'\theta'}$ and $\overline{v'\theta'}$ are of the same order of magnitude, although $\partial/\partial x \ll \partial/\partial y$. Hence, the KEM predicts a too low k-level, since $\overline{u'\theta'}$ appears in the G_k-term. This is shown in Fig. 12. All three models give nearly the same P_k-term. In the outer layer, the G_k-term attains values of about 30% of the P_k-term, which is not negligible.

6. CONCLUSIONS

The natural-convection boundary layer for air has been studied numerically with an RSM and an ASM. A suitable model was chosen from the literature. Sensitivity tests on all RSM constants show that C_1, $C_{1\theta}$ and wall constants C_{1w}, c_w are the most important parameters for the overall mean-flow and turbulence predictions. The other model constants have a much smaller effect on the mean flow or only control specific turbulence quantities. Wall-heat transfer predictions are sensitive to changes in most model constants, but u_{max} is hardly affected by variation of constants. The set recommended by refs. [5, 17, 37] was taken, but with $C_{1\theta} = 3.75$, $C_{1\theta w} = 0.75$ and $C_s = 0.20$. The selected set of constants was checked to give good mean-flow results.

Additional near-wall correction functions were included to account for the anisotropic dissipation rate close to the wall, thus establishing a correct near-wall behavior of turbulence quantities. The predicted turbulence quantities were compared with experiments. The ASM results agree qualitatively well with experiments of Tsuji and Nagano [7–9] and Miyamoto *et al.* [6], but RSM computations are superior to the ASM. Further, the calculations show that the local-

equilibrium assumption is not valid in the natural-convection boundary layer.

The inner layer structure is notably different from the outer layer. This is mainly due to the velocity gradient, which has opposite signs in the inner and outer layer. The data of Tsuji and Nagano suggest $\overline{u'v'} \approx 0$ and $\overline{u'\theta'} \approx 0$. Our numerical calculations, however, give $\overline{u'v'} < 0$ and $\overline{u'\theta'} < 0$. Better near-wall models are needed to improve predictions, but additional experimental data are useful as well, since the inner layer is very thin and accurate measurements are difficult.

The eddy-viscosity concept, employed in the KEM, does not give a realistic description of the turbulence structure. In particular, the turbulence is strongly anisotropic, in contrast with KEM assumptions. Moreover, turbulent transport normal to the mean gradient is underpredicted. As a result, a too low G_k-term is predicted by the KEM. Turbulent diffusion, described with an eddy-viscosity, is predicted correctly by the RSM, but the KEM gives only qualitative agreement with experiments. Furthermore, the turbulent Prandtl number σ_θ is certainly not a constant over the whole flow. Fortunately, mean-flow predictions do not suffer much from these shortcomings. Hence, the low-Reynolds-number KEM of Jones and Launder [2], Chien [3] or Lam and Bremhorst [4] will be suitable for most mean-flow predictions close to a solid wall. A fully differential RSM, however, is needed to predict correctly the detailed turbulence structure in the natural-convection boundary layer.

REFERENCES

1. R. A. W. M. Henkes and C. J. Hoogendoorn, Comparison of turbulence models for the natural convection boundary layer along a heated vertical plate, *Int. J. Heat Mass Transfer* **32,** 157–169 (1989).
2. W. P. Jones and B. E. Launder, The prediction of laminarization with a two-equation model of turbulence, *Int. J. Heat Mass Transfer* **15,** 301–314 (1972).
3. K.-Y. Chien, Predictions of channel and boundary layer flows with a low-Reynolds-number two-equation model of turbulence, AIAA-80-0134 (1980). Also *AIAA J.* **20,** 33–38 (1982).
4. C. K. G. Lam and K. Bremhorst, A modified form of the k–ε model for predicting wall turbulence, *J. Heat Transfer* **103,** 456–460 (1981).
5. W. M. To and J. A. C. Humphrey, Numerical simulation of buoyant turbulent flow—I. Free convection along a heated, vertical flat plate, *Int. J. Heat Mass Transfer* **29,** 573–592 (1986).
6. M. Miyamoto, Y. Katoh, J. Kurima and H. Kajino, An experimental study of turbulent free convection boundary layer along a vertical surface using LDV, *Proc. Osaka Symp. Flow-measuring Techniques*, Osaka, 15 July, pp. 83–104 (1983).
7. T. Tsuji and Y. Nagano, Characteristics of a turbulent natural convection boundary layer along a heated vertical flat plate, *Int. J. Heat Mass Transfer* **31,** 1723–1734 (1988).
8. T. Tsuji and Y. Nagano, Turbulence measurements in a natural convection boundary layer along a vertical flat plate, *Int. J. Heat Mass Transfer* **31,** 2101–2111 (1988).
9. T. Tsuji and Y. Nagano, Velocity and temperature measurements in a natural convection boundary layer along a vertical flat plate, *Expl Thermal Fluid Sci.* **2,** 208–215 (1989).
10. P. Y. Chou, On velocity correlations and the solutions of the equations of turbulent fluctuation, *Q. Appl. Math.* **3,** 38–54 (1945).
11. J. Rotta, Statistische Theorie nichthomogener Turbulenz, *Z. Phys.* **129,** 547–572 and **131,** 51–77 (1951).
12. M. S. Uberoi, Equipartition of energy and local isotropy in turbulent flows, *J. Appl. Phys.* **28,** 1165–1170 (1957).
13. J. Tucker and A. J. Reynolds, The distortion of turbulence by irrotational plane strain, *J. Fluid Mech.* **32,** 657–673 (1968).
14. J. L. Lumley, Computational modeling of turbulent flows, *Adv. Appl. Mech.* **18,** 123–176 (1978).
15. B. E. Launder, G. J. Reece and W. Rodi, Progress in the development of a Reynolds-stress turbulence closure, *J. Fluid Mech.* **68,** 537–566 (1975).
16. M. M. Gibson and B. A. Younis, Calculation of swirling jets with a Reynolds stress closure, *Physics Fluids* **29,** 38–48 (1986).
17. M. S. Hossain and W. Rodi, A turbulence model for buoyant flows and its application to vertical buoyant jets. In *Turbulent Buoyant Jets and Plumes* (Edited by W. Rodi), pp. 121–178. Pergamon Press, Oxford (1982).
18. B. E. Launder, On the effects of a gravitational field on the turbulent transport of heat and momentum, *J. Fluid Mech.* **67,** 569–581 (1975).
19. M. M. Gibson and B. E. Launder, Ground effects on pressure fluctuations in the atmospheric boundary layer, *J. Fluid Mech.* **86,** 491–511 (1978).
20. M. Ljuboja and W. Rodi, Prediction of horizontal and vertical turbulent buoyant wall jets, *J. Heat Transfer* **103,** 343–349 (1981).
21. M. M. Gibson and B. E. Launder, On the calculation of horizontal, turbulent, free shear flows under gravitational influence, *J. Heat Transfer* **98,** 81–87 (1976).
22. M. M. Gibson, W. P. Jones, J. J. McGuirk and J. H. Whitelaw, Turbulence models for computational fluid dynamics, Lecture Notes, Imperial College, London (1987).
23. K. Hanjalić and B. E. Launder, A Reynolds stress model of turbulence and its application to thin shear flows, *J. Fluid Mech.* **52,** 609–638 (1972).
24. B. J. Daly and F. H. Harlow, Transport equations in turbulence, *Physics Fluids* **13,** 2634–2649 (1970).
25. B. E. Launder, On the computation of convective heat transfer in complex turbulent flows, *J. Heat Transfer* **110,** 1112–1128 (1988).
26. A. Morse, Axisymmetric turbulent shear flows with and without swirl, Ph.D. Thesis, University of London (1980).
27. H. Tennekes and J. L. Lumley, *A First Course in Turbulence*. MIT Press, Cambridge, Massachusetts (1972).
28. A. S. Monin, On the symmetry properties of turbulence in the surface layer of air, *Izv. Akad. Nauk. SSR, Fiz. Atmos.* **11,** 45–54 (1965).
29. J. C. Wyngaard, Modelling the planetary boundary layer—extension to the stable case, *Boundary-Layer Met.* **9,** 441–460 (1975).
30. S. Tavoularis and S. Corrsin, Experiments in nearly homogeneous turbulent shear flow with a uniform mean temperature gradient. Part I, *J. Fluid Mech.* **104,** 311–347 (1981).
31. B. E. Launder, On the computation of convective heat transfer in complex turbulent flows, *J. Heat Transfer* **110,** 1112–1128 (1988).
32. J. C. Wyngaard and O. R. Coté, The evolution of a convective planetary boundary layer—a higher-order closure model study, *Boundary-Layer Met.* **7,** 289–308 (1974).
33. I. Dekeyser, Numerical predictions of an asymmetrical heated plane jet with a second-moment turbulence closure, *Int. J. Heat Mass Transfer* **28,** 653–662 (1985).

34. D. S. A. Samaraweera, Turbulent heat transport in two- and three-dimensional temperature fields, Ph.D. Thesis, University of London (1978).
35. W. P. Jones and P. Musonge, Modelling of scalar transport in homogeneous turbulent flows, *Proc. 4th Turb. Shear Flow Symp.*, Karlsruhe, F.R.G., pp. 17.18–17.24 (1983).
36. W. P. Jones and P. Musonge, Closure of the Reynolds stress and scalar flux equations, *Physics Fluids* **31,** 3589–3604 (1988).
37. Y. Nagano and C. Kim, A two-equation model for heat transport in wall turbulent shear flows, *J. Heat Transfer* **110,** 583–589 (1988).
38. B. E. Launder and D. S. A. Samaraweera, Application of a second-moment turbulence closure to heat and mass transport in thin shear flows—I. Two-dimensional transport, *Int. J. Heat Mass Transfer* **22,** 1631–1643 (1979).
39. C. Béguier, I. Dekeyser and B. E. Launder, Ratio of scalar and velocity dissipation time scales in shear flow turbulence, *Physics Fluids* **21,** 307–310 (1978).
40. Y. Nagano and M. Hishida, Production and dissipation of turbulent velocity and temperature in fully developed pipe flow, *Proc. 5th Symp. Turb. Shear Flows*, Cornell University, Ithaca, New York, pp. 14.19–14.24 (1985).
41. F. H. Champagne, V. G. Harris and S. Corrsin, Experiments on nearly homogeneous turbulent shear flow, *J. Fluid Mech.* **41,** 81–139 (1970).
42. C. C. Shir, A preliminary numerical study of atmospheric turbulent flows in the idealized planetary boundary layer, *J. Atmos. Sci.* **30,** 1327–1339 (1973).
43. K. Hanjalić and B. E. Launder, Contribution towards a Reynolds-stress closure for low-Reynolds-number turbulence, *J. Fluid Mech.* **74,** 593–610 (1976).
44. B. E. Launder and W. C. Reynolds, Asymptotic near-wall stress dissipation rates in a turbulent flow, *Physics Fluids* **26,** 1157-1159 (1983).
45. V. C. Patel, W. Rodi and G. Scheuerer, Turbulence models for near-wall and low-Reynolds number flows: a review, *AIAA J.* **23,** 1308–1319 (1985).
46. W. Rodi, A new algebraic relation for calculating the Reynolds stresses, *Z. Angew. Math. Mech.* **56,** 219–221 (1976).
47. S. Ostrach, An analysis of laminar free convection flow and heat transfer about a flat plate parallel to the direction of the generating body force, NACA Technical Note 2635 (1952).
48. W. K. George and S. P. Capp, A theory for natural convection turbulent boundary layers next to heated vertical surfaces, *Int. J. Heat Mass Transfer* **22,** 813–826 (1979).
49. H. Iacovides and B. E. Launder, ASM predictions of turbulent momentum and heat transfer in coils and U-bends, *Numerical Methods in Laminar and Turbulent Flow, Proc. 4th Int. Conf.*, Vol. 2, pp. 1023–1045. Pineridge Press, Swansea (1985).
50. M. M. Gibson and D. C. Leslie, The turbulent Prandtl number in the flow near a heated vertical surface, *Int. Commun. Heat Mass Transfer* **11,** 73–84 (1984).
51. R. Cheesewright and E. Ierokipiotis, Velocity measurements in a natural convection boundary layers, *Proc. 7th Int. Heat Transfer Conf.*, Munich, F.R.G., Vol. 2, pp. 305–309 (1980).

LE MODELE DE TENSION DE REYNOLDS DE LA TURBULENCE APPLIQUE A LA COUCHE-LIMITE DE CONVECTION NATURELLE LE LONG D'UNE PLAQUE VERTICALE

Résumé—On étudie numériquement la couche limite turbulente de convection naturelle d'air le long d'une plaque verticale avec un modèle algébrique (ASM) et un autre différentiel de tension de Reynolds (RSM). On sélectionne un jeu de constantes de façon à prédire le transfert thermique pariétal et la structure de l'écoulement moyen en bon accord avec l'expérience. Des tests de sensibilité sur les constantes RSM montrent quelles constantes dominent la prédiction de l'écoulement et quelles autres affectent seulement les grandeurs de la turbulence. Des modifications de paroi sont utilisées pour améliorer les prédictions de la turbulence proche de la paroi. Des calculs RSM des grandeurs de turbulence s'accordent bien avec les données expérimentales disponibles. Les résultats ASM sont moins bons mais néanmoins en accord qualitatif avec les expériences. Dans les couches limites de convection naturelle, l'hypothèse d'équilibre local n'a qu'une applicabilité limitée. En outre on teste le concept de viscosité turbulente utilisé dans le modèle k–ε. Celui-ci donne de bons résultats pour l'écoulement moyen mais pour une bonne prédiction de la structure détaillée de la turbulence on a besoin du RSM.

ANWENDUNG DES REYNOLDS'SCHEN SPANNUNGSMODELLS FÜR TURBULENTE STRÖMUNGEN AUF DIE GRENZSCHICHT EINER STRÖMUNG BEI NATÜRLICHER KONVEKTION AN EINER SENKRECHTEN PLATTE

Zusammenfassung—Die turbulente Grenzschicht bei natürlicher Konvektion in Luft entlang einer senkrechten beheizten Platte wird numerisch mit einem algebraischen (ASM) und einem differentiellen Reynolds'schen Spannungsmodell (RSM) untersucht. Aus der Literatur wird ein Satz von Modellparametern so ausgewählt, daß der Wärmeübergang an der Wand und die Struktur der Hauptströmung gut mit den Versuchsergebnissen übereinstimmen. Sensitivitätsuntersuchungen mit den Konstanten des RSM-Modells zeigen, welche Konstanten die Hauptströmung und welche nur die Turbulenzeigenschaften beeinflussen. Die Ergebnisse des RSM-Modells stimmen bezüglich der Turbulenzgrößen gut mit den vorhandenen Versuchsergebnissen überein. Die Ergebnisse des ASM-Modells sind schlechter, aber sie stimmen immer noch qualitativ mit den Versuchsergebnissen überein. Dies zeigt, daß die Annahme lokalen Gleichgewichts in der Grenzschicht von natürlichen Konvektionsströmungen nur begrenzt gültig ist. Weiterhin wird der Ansatz für die turbulente Viskosität untersucht, der im k–ε-Modell (KEM) verwendet wird. Das KEM liefert gute Ergebnisse für die Hauptströmung, für eine gute Beschreibung der Turbulenzvorgänge wird jedoch das RSM-Modell benötigt.

ИСПОЛЬЗОВАНИЕ МОДЕЛИ ТУРБУЛЕНТНОСТИ, ОСНОВАННОЙ НА НАПРЯЖЕНИИ РЕЙНОЛЬДСА, ДЛЯ ОПИСАНИЯ ЕСТЕСТВЕННОКОНВЕКТИВНОГО ПОГРАНИЧНОГО СЛОЯ ВДОЛЬ НАГРЕВАЕМОЙ ВЕРТИКАЛЬНОЙ ПЛАСТИНЫ

Аннотация—С использованием алгебраической (ASM) и дифференциальной модели рейнольдсовского капряжения (RSM) численно исследуется турбулентный естественноконвективный пограничный слой воздуха у нагретой вертикальной пластины. Результаты расчетов теплопереноса от стенки и структуры среднего течения, выполненных с использованием взятых из литературы параметров модели, очень хорошо согласуются с экспериментальными данными. Проверка точности дифференциальной модели рейнольдсовского напряжения показывает, какие из параметров являются доминирующими при определении среднего течения и какие оказывают влияние только на величины турбулентности. Для повышения точности расчетов турбулентности вблизи стенки используются ее различные варианты. Расчетные результаты для величин турбулентности, полученные с помощью модели RSM, хорошо согласуются с имеющимися экспериментальными данными. Результаты модели ASM менее точны, хотя и качественно согласуются с экспериментальными данными. Отсюда следует, что в случае естественноконвективных пограничных слоев применимость предположения о локальном равновесии ограничена. Также проверяется правомерность использования понятия турбулентной вязкости в модели k–ε (KEM). На ее основе получены удовлетворительные результаты по среднему течению, но для более точного определения детальной структуры турбулентности необходимо использовать модель RSM.